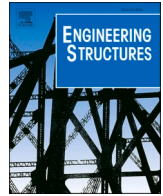


Contents lists available at [ScienceDirect](https://www.sciencedirect.com)

Engineering Structures

journal homepage: www.elsevier.com/locate/engstruct

Modelling imperfections in unreinforced masonry structures: Discrete element simulations and scale model experiments of a pavilion vault

Alessandro Dell'Endice^{a,*}, Antonino Iannuzzo^a, Matthew J. DeJong^b, Tom Van Mele^a, Philippe Block^a

^a ETH Zurich, Institute of Technology in Architecture, Zurich, Switzerland

^b UC Berkeley, Department of Civil and Environmental Engineering, Berkeley, CA, USA

ARTICLE INFO

Keywords:

Masonry structure
Discrete element modelling
Geometrical imperfections
Mechanical imperfections
Displacement capacity
Collapse mechanism
Pavilion vault
Flow of forces
Crack pattern

ABSTRACT

The structural assessment of doubly-curved vaulted masonry structures, such as pavilion vaults, poses challenges specific to their high degree of indeterminacy. Two-dimensional equilibrium analysis methods may provide a lower bound of load or displacement capacity, but they do not accurately describe the three-dimensional (3D) behaviour of these structures, particularly when shear deformation (e.g. sliding) is important. Therefore, discrete element modelling (DEM) methods, which can effectively simulate 3D load re-distribution, have been used to investigate support displacement capacity and corresponding 3D collapse mechanisms. DEM analyses are usually conducted on perfect digital geometries. Meanwhile, both real structures and small-scale physical models have implicit assembly and fabrication imperfections, which may significantly alter their response. The present paper aims to investigate the influence of geometrical and mechanical imperfections by comparing DEM analyses with the results obtained from tests on a scale model. In particular, a new method to simulate imperfections within the DEM framework is proposed, and a DEM parametric analysis is compared to the measured behaviour of a 3D-printed scale model of a pavilion (or cloister) vault on spreading supports. The influence of both mechanical imperfections and geometrical imperfections, due to element geometry deviations or imprecision of the assembly process, have been investigated. Based on these analyses, the three-dimensional behaviour of a pavilion vault subjected to horizontal displacement of the supports is described, and the variability of results due to imperfections is demonstrated. A good agreement between DEM analyses and 3D-printed scale model tests is achieved, in terms of crack patterns and mechanisms. Geometrical imperfections did change the load paths within the vault, as expected, and also influenced the displacement capacity.

1. Introduction

Despite the significant number of vaulted masonry structures throughout the world, there is still a lack of knowledge regarding their capacity to withstand support displacements, and computational simulation of structural response under large displacements is still a challenge. Many advanced mechanical methods, based on a large number of mechanical parameters, have been developed in recent years. The definition of these parameters requires an extensive characterization of the material. Meanwhile, even after an extensive survey, the intrinsic heterogeneity of masonry structures and of constructions techniques can lead to a large variability of responses which may limit the utility of extremely detailed mechanical models for practical assessment. For this reason, in order to avoid some of this uncertainty, scholars have focused

on the ultimate state of masonry structures by applying Limit Analysis. Many methods, based on Limit Analysis, have been developed, but their use for the assessment of 3D complicated geometries is still a challenge. In the last decades, the Discrete Element Method has been applied as a reliable way for the assessment of 3D geometries, using relatively few mechanical parameters. The next paragraphs will give an overview of existing methods and outline the remaining challenges in the assessment of unreinforced masonry vaulted structures.

1.1. Equilibrium analysis

In 1966, Heyman [1] defined Limit Analysis in the context of Unreinforced Masonry URM structures by formulating three fundamentals requirements for its application: masonry has infinite resistance in

* Corresponding author.

E-mail address: dellendice@arch.ethz.ch (A. Dell'Endice).

<https://doi.org/10.1016/j.engstruct.2020.111499>

Received 30 March 2020; Received in revised form 17 September 2020; Accepted 27 October 2020

0141-0296/© 2020 The Author(s). Published by Elsevier Ltd. This is an open access article under the CC BY-NC-ND license

(<http://creativecommons.org/licenses/by-nc-nd/4.0/>).

compression, no tensile strength, and infinite friction, that is, sliding cannot occur. The application of Limit Analysis leads to an important conclusion: the stability of URM structures depends on geometry rather than material strength. The oldest method for the assessment of URM structures that perfectly fits in the framework of Limit Analysis is Thrust Line Analysis (TLA). TLA is a powerful method that has been applied since the mid-1800's for investigating the stability of arches and vaults. Although this method describes the behaviour of two-dimensional structures very well [2,3], expedients such as the slicing technique have to be adopted to apply it to three-dimensional geometry. The downside of this procedure is that it does not capture the three-dimensional behaviour of the structure, e.g. in a dome, hoop forces cannot be taken into account [4]. For the analysis of fully 3D behaviour, other methods have been developed in the last decades, such as Thrust Network Analysis [5,6] or 2D compressed membranes [7–10]. Most of these methods are a computational application of the Safe Theorem, which means that they assess the stability through lower bound solutions: if at least one purely compressive singular “structure” can be found within the geometry, the structure is considered safe. In recent years, the piecewise rigid displacement (PRD) method, a novel energy-, displacement-based approach, has been developed by [11] to solve Limit Analysis problems for normal, rigid, no-tension materials following the Heyman hypotheses. It allows finding mechanisms and their corresponding internal stress states due to different boundary conditions [12] and to also perform displacement capacity analyses [13]. Beyond these approaches, Limit analysis methods discretising the masonry as an assemblage of interlocked blocks having interfaces with a finite friction capacity, have been developed [14–17].

1.2. Discrete element modelling

On the computational side, among the methods dealing with three-dimensional URM structures, the Discrete Element Modelling (DEM) method [18] has shown good results in the simulation of large displacements or collapse of masonry structures [19,20]. A DEM software has three main peculiarities: the model consists of finite-size bodies able to move and deform independently; large displacements are possible; the blocks can completely detach from each other, and new contacts between other blocks can form. The possibility of modelling rigid blocks with contact interfaces with no tensile strength, make this method suitable for URM structures. Moreover, as stated in [21], by using specific values for the mechanical parameters, DEM is suitable for approximating Heyman's assumptions [1]. Several works have been conducted using DEM to investigate the static and dynamic behaviour of masonry structures, [22–29]. The application of this method shows good results in the description of collapse mechanisms and displacement capacity. In [30] and [31], DEM analysis results have been compared with physical tests on 3D-printed models to investigate the dynamic behaviour of stone spires and to determine the displacement capacity and 3D

collapse mechanisms of a cross vault under differential support displacements, respectively. Recently also, other DEM approaches have been developed using macro-elements and non-linearity conditions at the interfaces to model masonry structures [32,33].

1.3. Scale models

The use of physical scale models was one of the first methods historically applied (e.g. tests made by Danyzy in 1732 [34] and reported later in Frèzier 1737–39 [35]). Particularly when the complexity of the building project increases, architects and engineers have used scale models to demonstrate the feasibility of the project, the assembly sequence or the general behaviour of the structure [36]. Since stability of URM structures is predominantly a problem of geometry rather than stress, scale models well approximate the behaviour of actual structures for the assessment of the level of stability, for the investigation of three-dimensional collapse mechanisms, or for predicting the displacement capacity of a structure under given foundation settlements. The only concerns related to physical models refer to the non-scalability of the effect of friction and the necessary simplification of the stereotomy. In recent years, the advent of new technologies for their fabrication has changed the use of scale models considerably. Digital design and fabrication allow the design and construction of complex geometries in a short amount of time and with a limited budget. Additive manufacturing such as 3D printing makes the fabrication of scale models cost efficient, fast and flexible. The same model can be re-used for several tests (e.g. [30]), and it can be easily combined with other tools as optical measurement systems [31,37] or force sensitive robotic arms for a more advanced testing setup [38] (Fig. 1).

1.4. Geometrical and mechanical imperfections

Physical models are not only useful for understanding the collapse mechanisms and the fully three-dimensional behaviour of URM structures, but also for calibrating computational tools such as DEM. Physical scale models, as well as full-scale structures, contain geometrical imperfections, which can be due to fabrication deviations, assembly errors during construction, or damages. Imperfect contacts lead to a different type of interaction between adjacent blocks, which influences the internal stress state, that is impossible to find precisely [39]. Moreover, especially in historical buildings, mechanical parameters such as the friction angle are not homogeneous throughout the structure. Very often, virtual models tested with computational tools represent a “perfect” version of the structural geometry with no imperfections, neither geometrical nor mechanical, and the role of imperfections has not been extensively investigated. However, it has been shown that the flow of forces can change within a structure due to non-perfect contact conditions and due to the mechanical parameters of the material. For example, photo-elastic analysis of a scale model of a masonry wall

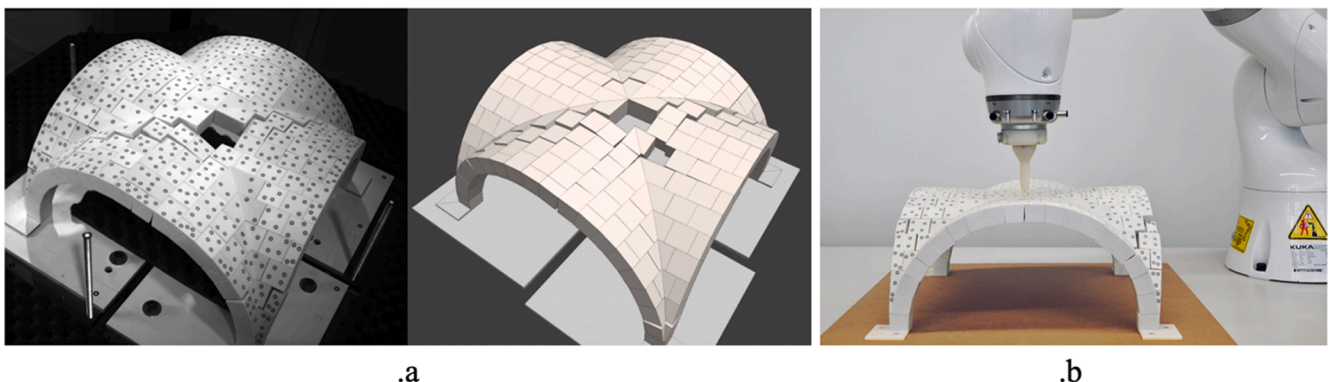


Fig. 1. (a) Physical model (left) and digital model (right) in [31]. (b) Point load test with a force-sensitive robot in [38].

subject to a vertical point load was used to demonstrate a load percolation phenomenon [40,41]. Specifically, in case of low external applied load, the forces are localised because they are transferred throughout points contact between the blocks (Fig. 2a). Only by increasing the load value, because of the mechanical parameters of the material used in the test, the contact points become contact areas, and the load distributes more uniformly (Fig. 2.b). In the case of unreinforced masonry, the material is relatively stiff, the working stress is relatively low compared to the strength of the material, and thus, the deformation is much smaller, which reduces the load redistribution.

Similarly, the influence of geometrical imperfections due to material production tolerances has been investigated for concrete blocks of a dry-stacked masonry wall [42]. The results show that imperfections lead to localisation of the flow of forces, resulting in a non-homogeneous distribution of the stresses.

1.5. Structural behaviour of a pavilion vault

Few studies have addressed the structural behaviour of pavilion vaults. In [43] a detailed study has been conducted comparing different methods: a non-linear finite element analysis, an approach based on limit analysis, membrane theory considering unilateral material and a 2D approach considering the pavilion vault as an assembly of 2D arches. The main results of this comparison are: the horizontal thrust of a pavilion vault on the supports is almost constant along the perimeter, and tension forces along the bottom part of the diagonals and the webs are responsible for the pavilion vault's typical crack pattern, which means that cracks can not be traced back to the support displacements. Moreover, [43] shows that a 2D analysis of a pavilion vault, results in a triangular distribution of the horizontal thrust on the supports, completely ignoring the thrust in correspondence of the diagonals (Fig. 3).

1.6. Objectives

Comparisons between physical tests and computational models are useful to validate DEM tools and to calibrate mechanical parameters used in the analyses. Although such comparisons have already been conducted, the influence of the imperfections due to fabrication and assembly errors has not yet been addressed. This discrepancy among physical and digital model could cause mistakes in understanding the behaviour of real structures. This paper, therefore, investigates the importance of mechanical and geometrical imperfections on the

behaviour of a pavilion vault in terms of force distribution, displacement capacity and collapse mechanisms. This is achieved in two steps: 1) comparison of the results of [37] on a physical model of a generic pavilion vault subject to horizontal displacements of the supports with a computational analysis conducted on a numerical model of the same geometry using the DEM software 3DEC by Itasca [44–46]; 2) investigation of the influence of mechanical and geometrical imperfections on the structural behaviour and displacement capacity. In the current work, an entire pipeline to generate imperfect digital models and analyse them has been implemented.

2. Methodology

The analysis carried out in this paper started with the comparison of the 3D-printed scale model studied in [37] with its digital version tested using 3DEC. The digital model considered in this phase had perfect geometry (i.e. blocks have perfect straight edges and planar surfaces, resulting in perfect face-to-face contact conditions between them), and the same friction angle value was assigned to all the blocks. Then, mechanical imperfections were applied, considering a stochastic distribution of the friction angles assigned to the voussoirs (see 2.3.1). Finally, the influence of geometrical imperfections due to material fabrication and assembly errors was investigated (see 2.3.2). The whole analysis has been preceded by a sensitivity analysis to investigate the influence of the joint stiffness in the 3DEC calculation, as described in more detail in Section 2.4. The analyses performed have been implemented in COMPAS, an open-source, Python-based, framework developed at ETH Zurich for research and collaboration in architecture, engineering, fabrication and construction [47]. The main library of COMPAS provides flexible data structures, a geometry processing library, numerical solvers and other components as a base framework for computational research. Moreover, several additional COMPAS packages provide tools for processing, visualising and interacting with datastructures. Indeed, the meshes created in [37] using the CAD software Rhinoceros® have been translated in COMPAS meshes using the package *compas_assembly*, which provides tools for the generation of assemblies of discrete elements and for the management of the relationships between the individual parts. After this step, the geometry can be fully managed, and operations, such as the introduction of imperfections, are made possible. Once the geometry is ready, files readable by 3DEC have been created. These files contain all the information needed to set up a model and run an analysis in 3DEC: not only geometric data and material properties are stored but also boundary conditions including loads and (applied) displacements. In this step, mechanical imperfections are generated. During the analysis, at each step of the calculation, custom 3DEC functions store all model information and results. After the analysis, these results have been post-processed: the resultant contact forces at each interface

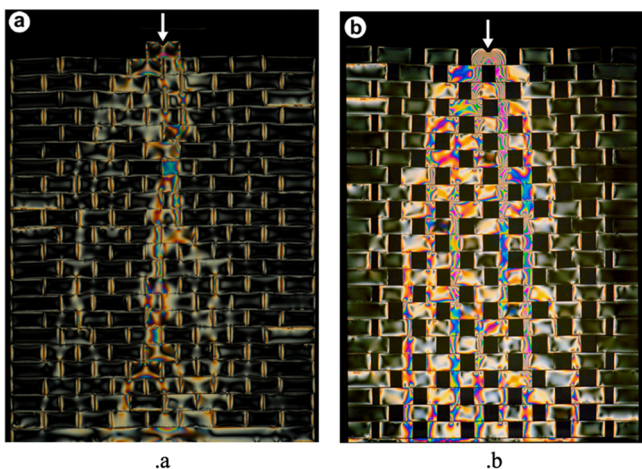


Fig. 2. Image taken from [40]. Photoelastic fringes of a model of dry masonry with thin vertical joints detected with a linear transmission polariscope. In (a) low vertical load of 125 N. (b) High vertical load of 400 N. For further details, the reader is referred to [40].

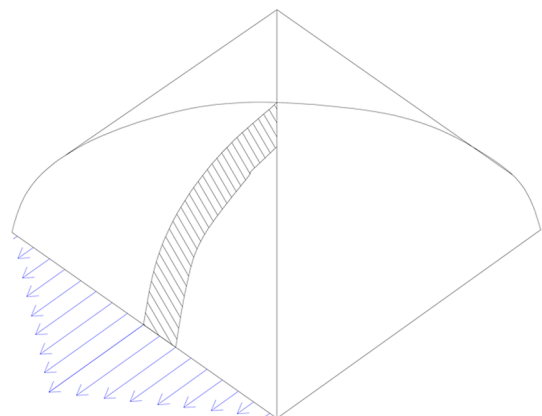


Fig. 3. Image taken from [43]. Horizontal thrust on the support calculated using 2D analysis. For further details, the reader is referred to [43].

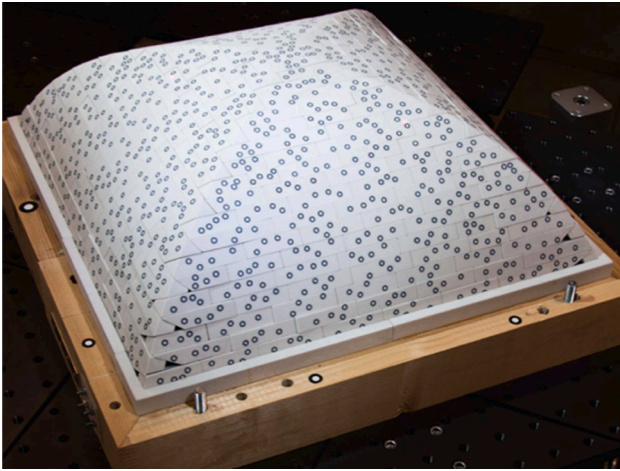


Fig. 4. Physical model of the 3D printed pavilion vault tested in [37].

between blocks have been computed, and the flow of forces within the structure visualised.

2.1. Description of the physical model

The reference model for this study is the pavilion vault of [37]. The vault has a square base, an internal span of 343 mm, a rise of 111 mm, and a constant thickness of 12 mm (Fig. 4). The vault's pattern is characterised by a shift of half a block between consecutive courses. The average dimensions of the blocks are $12 \times 12 \times 48$ mm except for the ones close to the edges, which have a particular stereotomy. For the physical collapse tests in [37], all the blocks had been printed with the ZPrinter 650 by 3D Systems having a printer tolerance of 0.1 mm. The material used is the zp151 powder, and the infiltration product is the Z-Bond 90. According to the 3D Systems ZPrinter Consumables Catalogue, a 3D-printed part made out of zp151 and infiltrated with Z-Bond 90 has Young's modulus equal to 9450 MPa. This value has been used for the calculation of the joint stiffness in the 3DEC analysis. The material's density was equal to 1460 kg/m^3 . The friction angle has been measured using an inclined testing table on more than 60 blocks. The average value found is 45° with a standard deviation of $\pm 9^\circ$ (20%). The tests performed in [37] consisted of the spreading of the supports of the pavilion vault scale model, obtained by the movement of three plates of a modular testing table, controlled by an actuator in displacement control.

The tests were quasi-static, and the applied velocity was 0.6 mm/s. In [37], different types of horizontal displacements have been simulated: symmetric displacement involving half, one quarter and one eighth of the supports (see Fig. 5) and also displacements involving asymmetric part of the supports. In this paper, only the symmetric displacements of

the supports have been simulated in the numerical model.

2.2. Digital model and computational DEM analysis setup

The digital model of the pavilion vault was converted to a numerical model and analysed with the commercial DEM software 3DEC by Itasca. The voussoirs have been modelled as rigid with dry joints. Because of these hypotheses, only four parameters need to be specified: the material density, friction angle, and the two values of the joint stiffness (described in detail in 2.4). As mentioned in 2.1, the material density is equal to 1460 kg/m^3 , and the average friction angle measured is 45° with a standard deviation of $\pm 9^\circ$. Gravity has been applied gradually in ten steps to avoid dynamic effects. The velocity used for simulating the displacements of the supports is the same as in [37], 0.6 mm/s. The displacements have been applied in small increments of 0.6 mm. After each step, the velocity of the support was set to 0.0 mm/s, and the equilibrium calculation ran for two seconds in order to dissipate the effects of support movement in the static structure. During the application of the gravity load, viscous damping has been used to absorb the vibrational energy as rapidly as possible. The vibrational energy is absorbed in proportion to the rate of change of kinetic energy [46]. For the simulation of the supports' displacement, a non-viscous energy dissipation has been applied. This type of damping is appropriate for quasi-static analysis because it applies a damping force to the blocks not proportional to the velocity, but to the unbalanced force [48]. For all the computational analyses conducted, the detection of the collapse step in 3DEC has been done by plotting the "out of balance" forces, computed by 3DEC, per block at each step of the calculation. Each voussoir has been plotted with a colour related to the magnitude of its out of balance force.

2.3. Imperfections

To understand the influence of imperfections on the structural behaviour of the pavilion vault, geometrical and mechanical imperfections have been generated on the digital model. Mechanical parameters in real structures are not homogeneous for two main reasons: variation in the materials used for the construction, especially in historical URM buildings, and imperfections at the interfaces that could change the contact conditions. Geometrical imperfections are due to material production errors, mistakes in the placement during the assembly and construction, or to damages.

2.3.1. Mechanical imperfections

Usually, the friction angle in discrete element analyses is applied as a single value to all elements of the model. In this work, analyses are performed using non-uniform distributions of the friction angle to understand the influence, on the structural behaviour, of uncertainty about the material properties in real structures. Friction angles have been

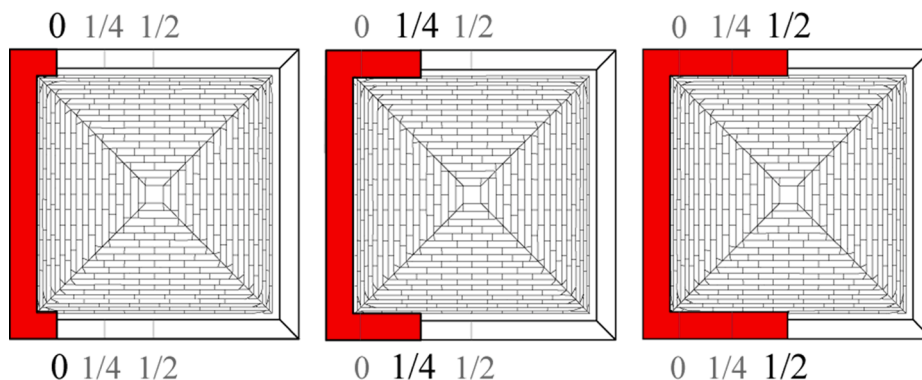


Fig. 5. The three symmetric support displacements in [37] tested in this paper through DEM analysis.

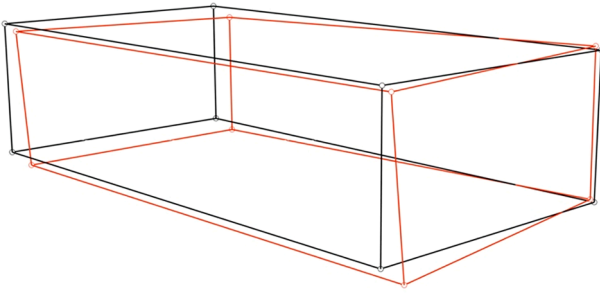


Fig. 6. Example of fabrication imperfections generation: in black, the perfect voussoir and in red the modified geometry: just for clarity, in this figure, the red block has been modified with a deviation, multiplied by a factor 10 (± 10 mm), than the one used for the analyses. (For interpretation of the references to colour in this figure legend, the reader is referred to the web version of this article.)

assigned randomly from uniform distributions around 45, within ranges of $\pm 10\%$, 20% , or 30% .

2.3.2. Geometrical imperfections

Geometrical imperfections from material fabrication and assembly errors have been generated on the digital model as well. Fabrication errors are chosen in relation to the 3D printer tolerance, which is equal to 0.1 mm. For each block, a random deviation in the range of ± 0.1 mm is added to the coordinates of every vertex. Fig. 6 shows an example of a block before and after the application of fabrication errors. The imperfections due to assembly errors have been generated by translating each block in the direction of one of its face normal directions (Fig. 7). A range for the translation displacement has been generated considering $\pm 2\%$ of the largest block dimension ($\pm 2\%$ of 48 mm). In this paper, the digital model has been analysed first applying only printer tolerance

imperfections and then adding on top of that assembly imperfections.

2.4. Sensitivity analysis on the joint stiffness

At the beginning of this work, a sensitivity analysis has been conducted to study the effects on the displacement capacity of parameters needed by 3DEC to perform the calculation, such as the two joint stiffness values (normal and shear). According to [20], the joint stiffness values should be specified as high as possible in order to reduce joint deformations (penetration and sliding between voussoirs), but the use of high values significantly increases the calculation time and presumes the existence of perfectly planar and smooth joints. On the other hand [31], shows that a reduction of the joint stiffness values by ten times does not significantly affect the results in the case of a digital model of a cross vault, but it considerably decreases the calculation time. In the case of the cross vault in [31] or for the structure examined in the present paper, geometry plays an essential role in the stability. A reduction of the joint stiffness values physically means allowing penetration and sliding between blocks. Nevertheless, since the starting values of the joint stiffnesses are high, and their reduction is relatively small, the effect of decreasing them, inside certain limits, does not affect the stability significantly. In addition, smaller values are more representative in the case of reduced contact area due to imperfections and roughness of the joints. Regarding the relation between joint stiffness and calculation time, as explained in [46], the magnitude of the time steps used by 3DEC for the analysis is inversely proportional to the joint stiffness values. Hence, a reduction of the joint stiffness values increases the magnitude of the timesteps, which results in fewer calculation cycles needed by 3DEC to complete the analysis. The value of the normal joint stiffness has been evaluated as in [26]:

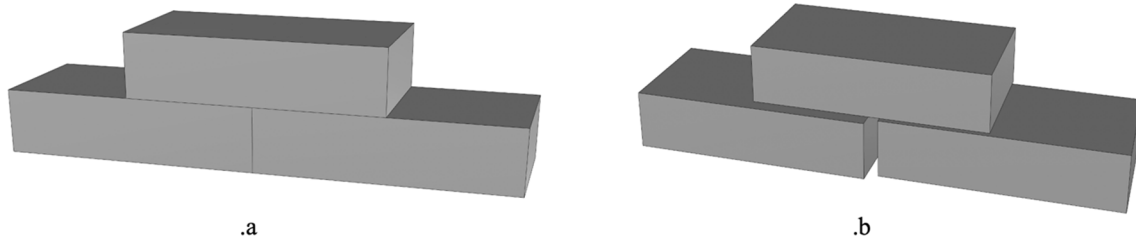


Fig. 7. Example of assembly imperfections generation: (a) perfect assembly, (b) imperfect assembly after the translation of the blocks.

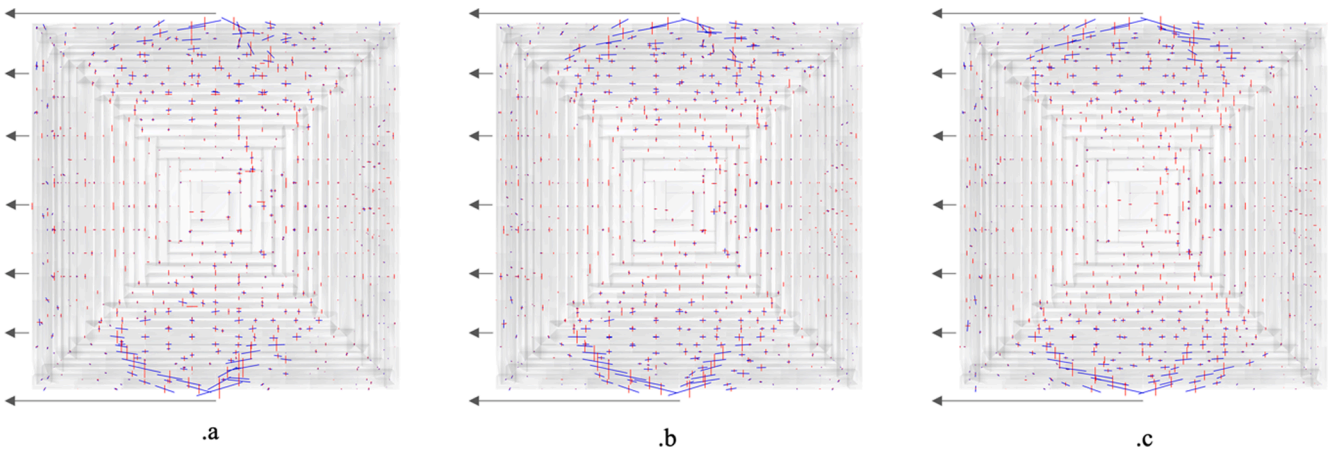


Fig. 8. Displacement of $\frac{1}{2}$ of the support. Normal (in red) and shear (in blue) components of the contact forces after one step displacement (0.6 mm) in the direction of the grey arrows. (a) joint stiffness equal to the calculated value, (b) calculated value multiplied by $\frac{1}{8}$, (c) calculated value multiplied by $\frac{1}{16}$. (For interpretation of the references to colour in this figure legend, the reader is referred to the web version of this article.)

Table 1

Displacement capacity values: in the second column the results from the 3D-printed model in [37]; in the third column the results of the analyses on the perfect digital model in 3DEC; in the fourth column the variation between 3DEC analyses and physical tests in [37].

Test (support displacement)	Results from [37]	3DEC analysis with perfect digital geometry	Variation
1/2	2.72%	2.90%	+0.18%
1/4	2.82%	3.58%	+0.76%
1/8	2.65%	3.58%	+0.93%

$$J_{kn} = \frac{\left(\frac{E}{h_{block}} + \frac{E}{l_{block}} \right)}{2} \quad (1)$$

where J_{kn} is the normal joint stiffness, E is the Young's modulus of the material, h_{block} and l_{block} are respectively the average block height and block length. To understand the effect of the reduction of the joint stiffness values, in the case of the structure analysed in this paper, the digital, perfect geometry has been analysed considering the two joint stiffness values reduced by five different scaling factors: starting from the joint stiffness value calculated as shown in Eq. (1), the model was tested scaling the joint stiffness values by 0.5, 0.25, 0.125 and 0.0625.

For the evaluation of the joint shear stiffness, the E (Young's modulus) has been replaced by G (shear modulus). Because no data is

available on the value of G of the 3D-printing material, it has been evaluated as

$$G = \frac{E}{2(1 + \nu)} \quad (2)$$

where ν is the Poisson's coefficient considered equal to 0.2.

Then, the value of the shear joint stiffness has been evaluated as in [26]:

$$J_{ks} = \frac{\left(\frac{G}{h_{block}} + \frac{G}{l_{block}} \right)}{2} \quad (3)$$

The reduction of the joint stiffness values, normal and shear, from the values calculated to 1/16 did not show a significant effect on the displacement capacity, and it did not result in interpenetration phenomena or considerable sliding. Fig. 8a–c show the influence of the reduction of the two joint stiffness values on the normal (in red) and shear (in blue) components of the contact forces, after one step of the displacement (0.6 mm), in the case of displacement of 1/2 of the support and friction angle equal to 45. A reduction of the joint stiffness by a factor of 16 did not cause any significant variation in the distribution of the contact forces. Meanwhile, from a computational point of view, this reduction showed a positive effect related to the calculation time, which decreases by almost 85%. For this reason, in this paper, the analyses with mechanical imperfections employ a joint stiffness reduction factor

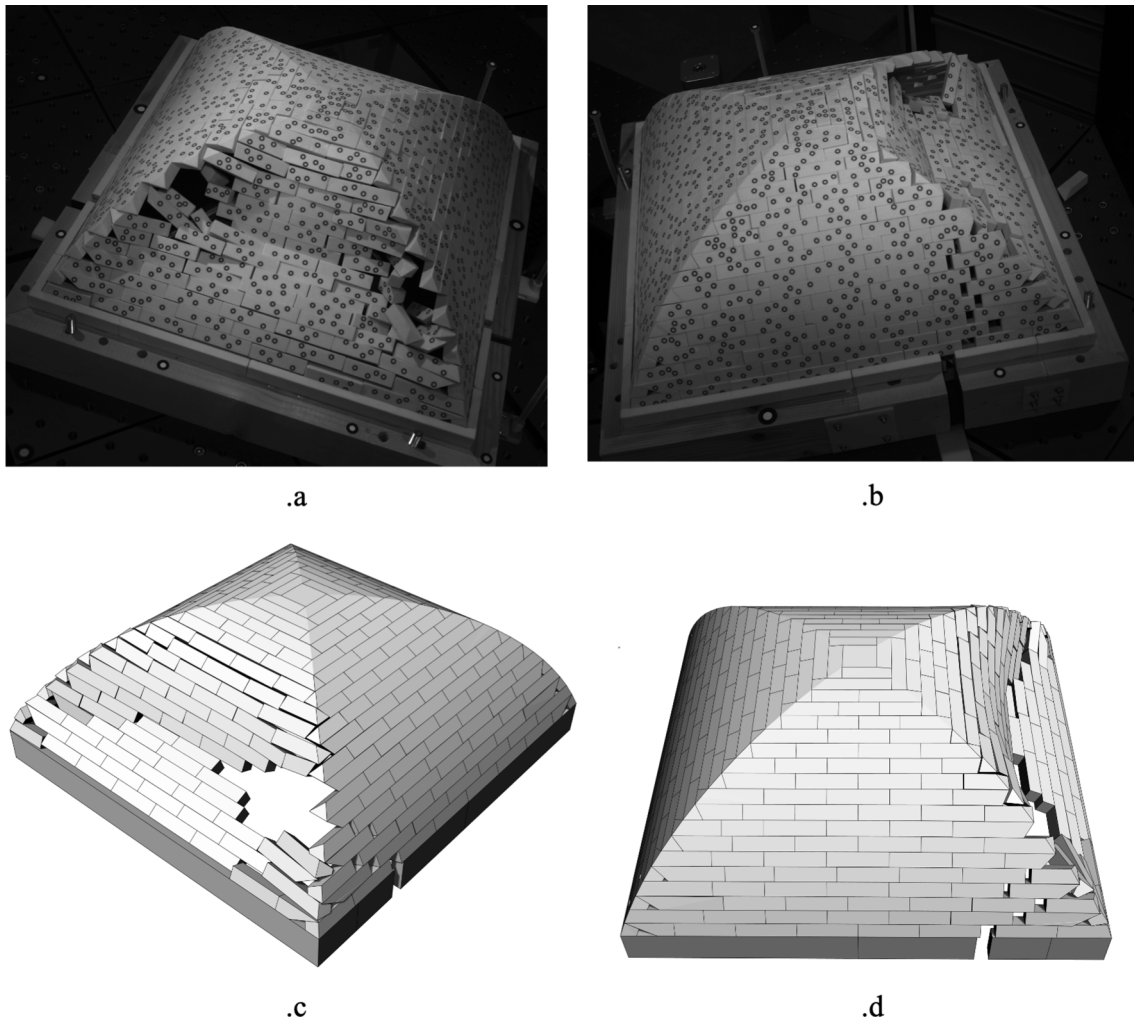


Fig. 9. Horizontal displacement of 1/4 of the support: (a) and (b) front view and lateral view of the physical model [37], (c) and (d) front view and lateral view of the digital model in 3DEC.

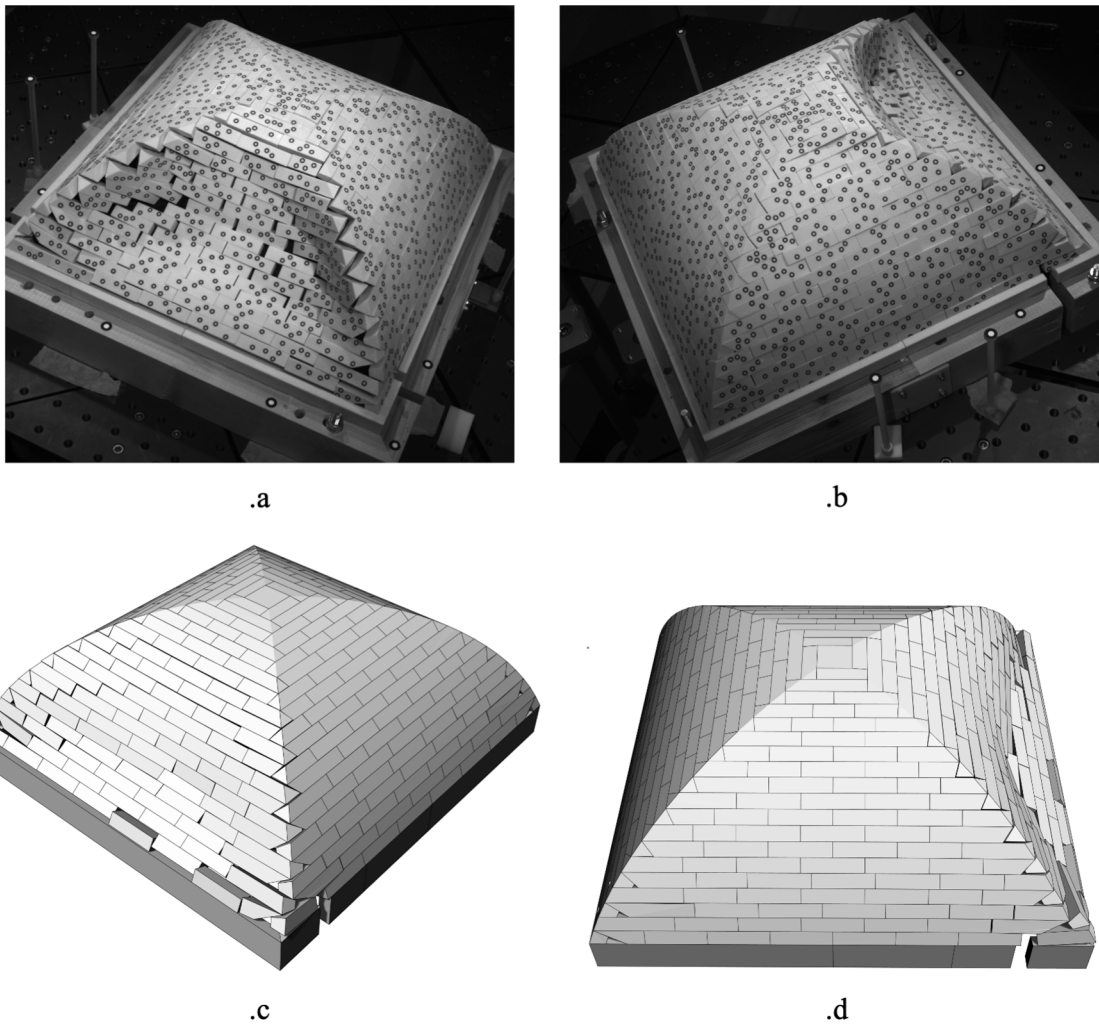


Fig. 10. Horizontal displacement of $\frac{1}{8}$ of the support: (a) and (b) front view and lateral view of the physical model [37], (c) and (d) front view and lateral view of the digital model in 3DEC.

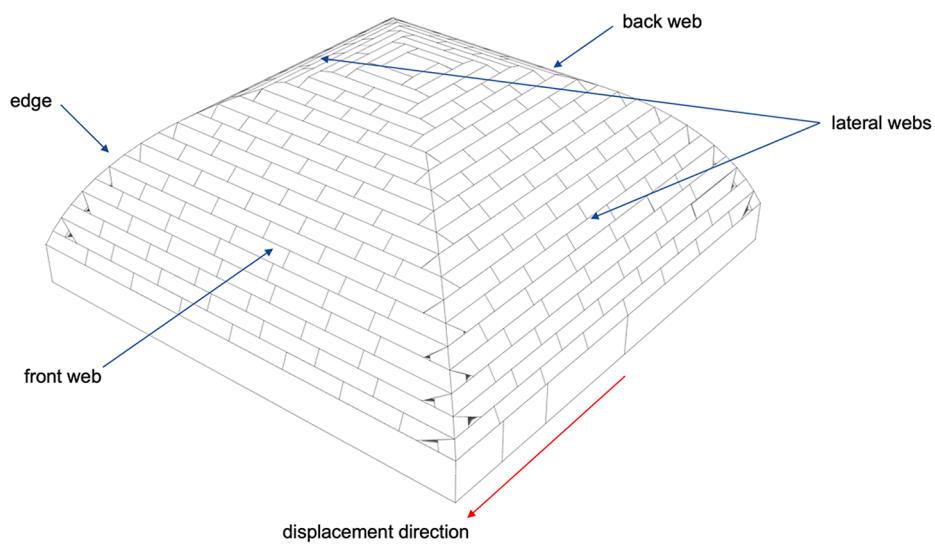


Fig. 11. Digital model used for the comparison with [37]. This figure shows the terminology used in the description of the tests and the direction of the displacement applied.

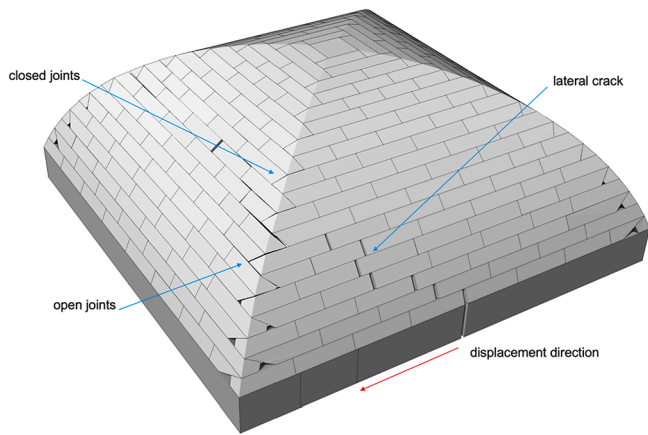


Fig. 12. Digital model with perfect geometry after a displacement equal to 0.85% of the vault's span.

of 8, while the analyses with geometrical imperfections employ a joint stiffness reduction factor of 16.

3. Results: perfect digital model

In this section, the results related to the perfect digital model of the pavilion vault will be described and discussed. In 3.1, the results of the comparison with the analyses conducted in [37] on the physical model will be presented. In the sub-section 3.1.1, the structural behaviour and the three-dimensional mechanism observed during the support displacement until the collapse of the perfect digital geometry will be described.

3.1. Comparison with the physical model

In Table 1, a comparison between the displacement values in [37] and those obtained from the tests performed in 3DEC on the perfect digital geometry, with friction angle equal to 45° and joint stiffness values calculated as in (1,3) is reported. The percentages provided in Table 1 correspond to the ratio between the ultimate displacement at collapse and the vault's span.

The values in Table 1 show that the ultimate displacement capacity measured in the numerical model is quite similar to the one described by [37] for each of the three support displacements. With regards to the slight variation, it is worth saying that to identify the collapse in this paper and in [37], two different approaches were used. In [37], the ultimate displacement is judged during the test on the testing table with the help of an optical measuring system. In 3DEC the collapse was

detected when the unbalanced forces of the voussoirs were not equal to zero. From a qualitative point of view, the comparison between the numerical 3DEC model with perfect geometry and the results in [37] showed a good agreement in terms of crack patterns and collapse mechanisms. Both models showed similar typological behaviour for each type of supports displacement (i.e. $\frac{1}{2}$, $\frac{1}{4}$, $\frac{1}{8}$). Only small differences can be seen on the location of the hinges just before the collapse. The following figures (Fig. 9a–d, Fig. 10a–d) compare the collapse of the physical model with the collapse observed in the digital simulation.

3.2. Three-dimensional behaviour of a pavilion vault subject to horizontal displacement of the supports

In this section, the three-dimensional structural behaviour of (the digital model of) a pavilion vault subjected to horizontal displacement of the supports will be described. Fig. 11 shows the terminology adopted to describe the different parts of the model.

All the analyses conducted showed that as soon as the support starts moving horizontally, two cracks, one per side, on the lateral webs, appear. These cracks propagate from the location where the support starts splitting to the edge of the vault (Fig. 12). The horizontal displacement would cause a diagonal crack on the lateral web, but the geometry of the crack is influenced by the stereotomy of the vault (staggered pattern).

Once the lateral cracks propagate and reach the front web, the vault's edges could be considered split into two parts, a bottom and an upper part. The joints, in the bottom part, open immediately because the displacement due to the opening of the crack is transferred to the edge bottom part, while the joints on the upper part only open as we get closer to collapse (Fig. 12). The visualization of the flow of forces highlights the increment of shear forces at the voussoirs' interfaces of the lateral web due to the horizontal displacement of the support (Fig. 13), causing the sliding in that area. In the analyses, the Mohr-Coulomb failure criterion is adopted:

$$\tau = \sigma \tan(\phi) + c \quad (4)$$

where τ is the shear strength, σ is the normal stress, ϕ is the friction angle and c the cohesion. In the numerical analyses conducted, a non-cohesive behaviour of the interfaces has been assumed, thus the cohesion was specified to be zero.

At the interfaces, where the maximum value of the shear strength is reached, cracks open. The achievement of the maximum value of the shear strength is related to the magnitude of the normal stress acting on the interface. In each course, the distribution of the normal forces varies in relation to the stereotomy, that is, to the offsetting of the blocks (Fig. 13).

Regarding the front web, once the horizontal displacement of the

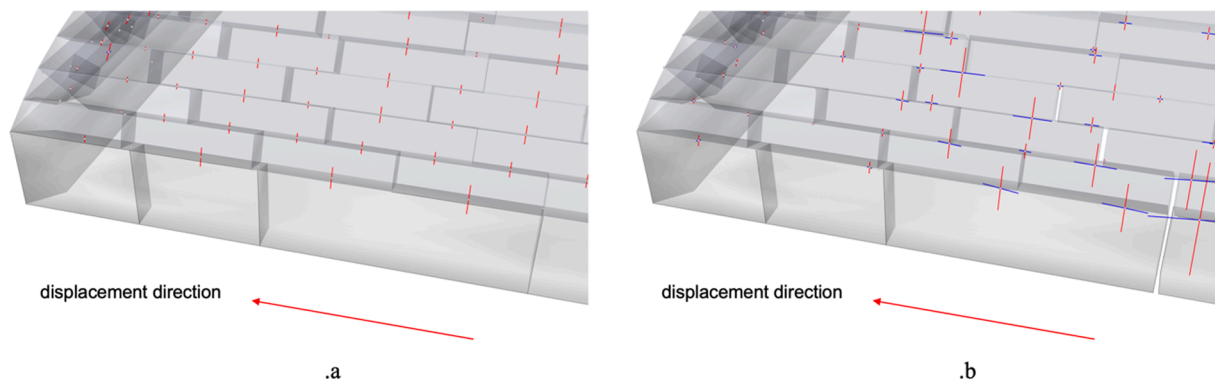


Fig. 13. Normal components in red and shear components in blue of the contact forces in the numerical model. (a) numerical model subject to self-weight, (b) numerical model after a displacement equal to 0.85% of the vault's span. (For interpretation of the references to colour in this figure legend, the reader is referred to the web version of this article.)

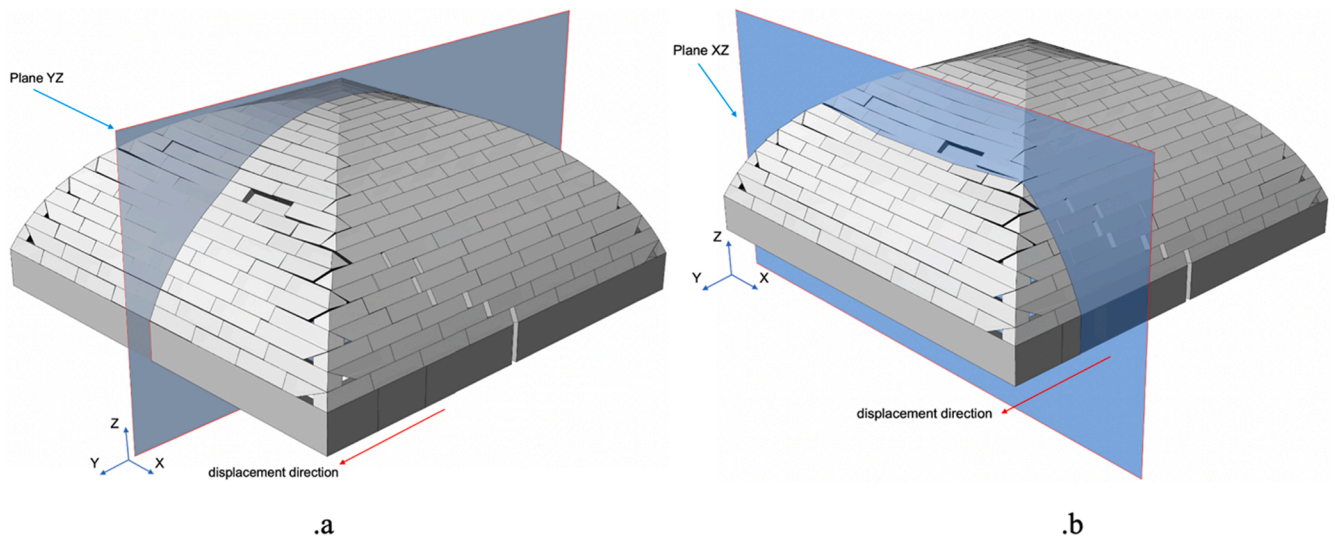


Fig. 14. Numerical model after a displacement equal to 1.7% of the vault's span. (a) plane YZ, (b) plane XZ.

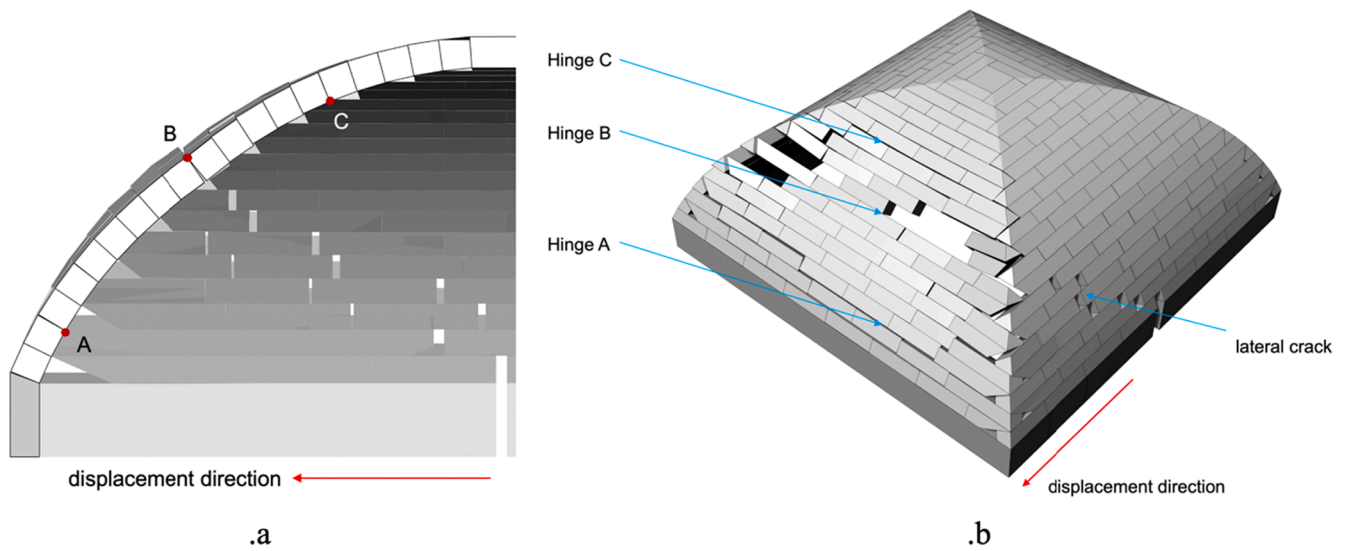


Fig. 15. (a) section in the plane YZ, the red dots show the position of the hinges. (b) Positions of Hinge A, B and C after a displacement equal to 3.07% of the vault's span. (For interpretation of the references to colour in this figure legend, the reader is referred to the web version of this article.)

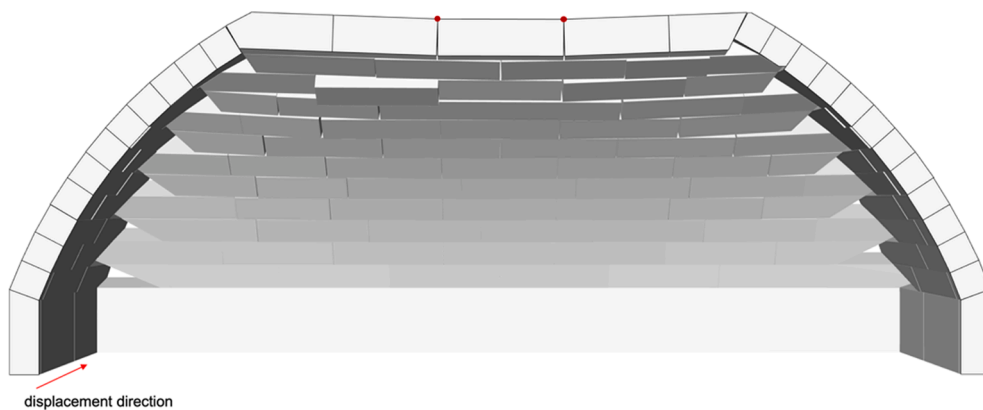


Fig. 16. Section on the plane XZ, the red triangles show the position of the hinges. (For interpretation of the references to colour in this figure legend, the reader is referred to the web version of this article.)

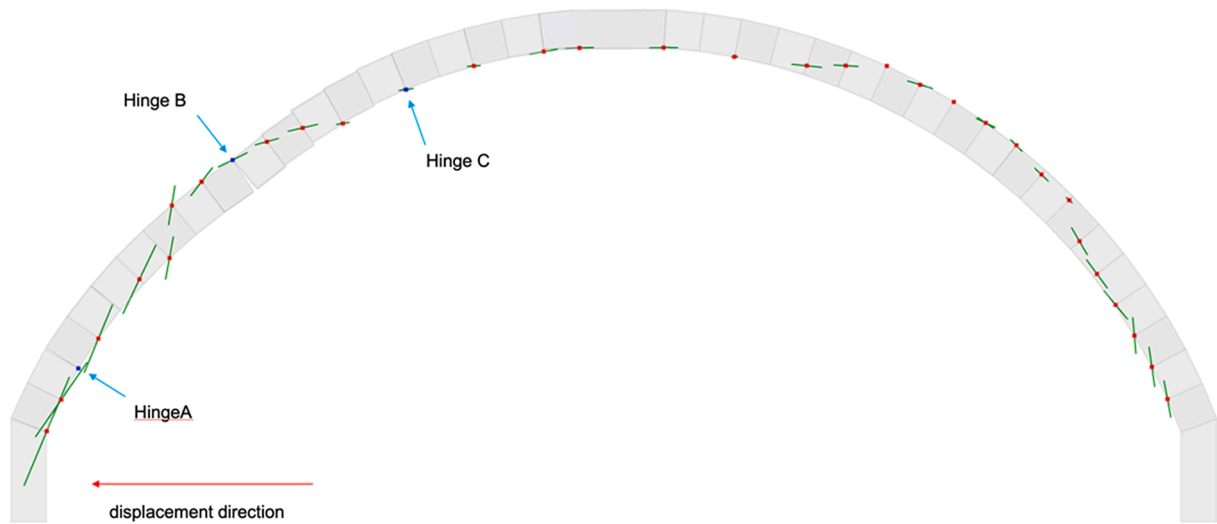


Fig. 17. Contact forces in the plane YZ. Contact forces and hinges position in the plane YZ with the displacement of $\frac{1}{2}$ of the support.

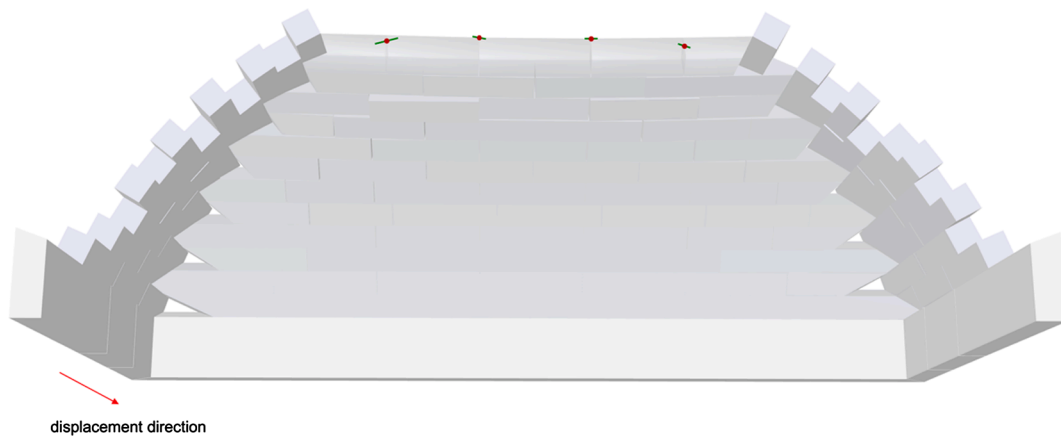


Fig. 18. Contact forces in the plane XZ. Contact forces in a horizontal row of the front web after seven displacement steps.

support starts, the voussoirs move in the negative z-direction, and a three-dimensional behaviour connected to the cracks on the lateral webs has been observed. For clarity, we describe the three-dimensional mechanism in two different planes, YZ and XZ, as shown in (Fig. 14a,b).

In the plane YZ (Fig. 15a), the structure behaves as an arch on spreading supports with a three-hinges mechanism. The hinge B in the central area of the front web is located along the line connecting the two points where the lateral cracks touch the edges. Hinge A and Hinge C (Fig. 15b) are respectively at the bottom and the top of the front web. This observation is in contrast with what was concluded by [37], where only hinge A was considered to be influenced by the lateral cracks.

In the plane XZ, the horizontal courses of voussoirs start behaving as a horizontal discretised “beam”, i.e. a flat arch, supported at the ends. The deflection of these horizontal elements in the negative z-direction causes the opening of cracks on the intrados and at the edges (Fig. 16).

The combination of the two phenomena causes small amounts of sliding during the collapse. The observation of the flow of forces clarifies both behaviours. In the plane YZ, the resultants of the contact forces at the interfaces touch the boundaries of the vault thickness in the three points which correspond to the hinges A, B and C (Fig. 17). Increasing the horizontal displacement of the support will increase the opening of the hinges until the collapse.

In the XZ plane, (Fig. 18), the voussoirs are touching each other only in the upper part, transferring compression forces horizontally to the lateral webs. When the displacement increases, at the points where the

Table 2

Results of the 3DEC analyses conducted on the numerical model with perfect geometry and mechanical imperfections.

Test (support displacement)	Friction angle range	Displacement capacity	Variation compared to [37]	Variation compared to perfect digital geometry
1/2	45° +/-10%	3.24%	+0.52%	+0.34%
1/2	45° +/-20%	3.41%	+0.69%	+0.51%
1/2	45° +/-30%	3.24%	+0.52%	+0.34%
1/4	45° +/-10%	3.24%	+0.42%	-0.34%
1/4	45° +/-20%	3.24%	+0.42%	-0.34%
1/4	45° +/-30%	3.24%	+0.42%	-0.34%
1/8	45° +/-10%	3.58%	+0.93%	0.0%
1/8	45° +/-20%	3.58%	+0.93%	0.0%
1/8	45° +/-30%	3.58%	+0.93%	0.0%

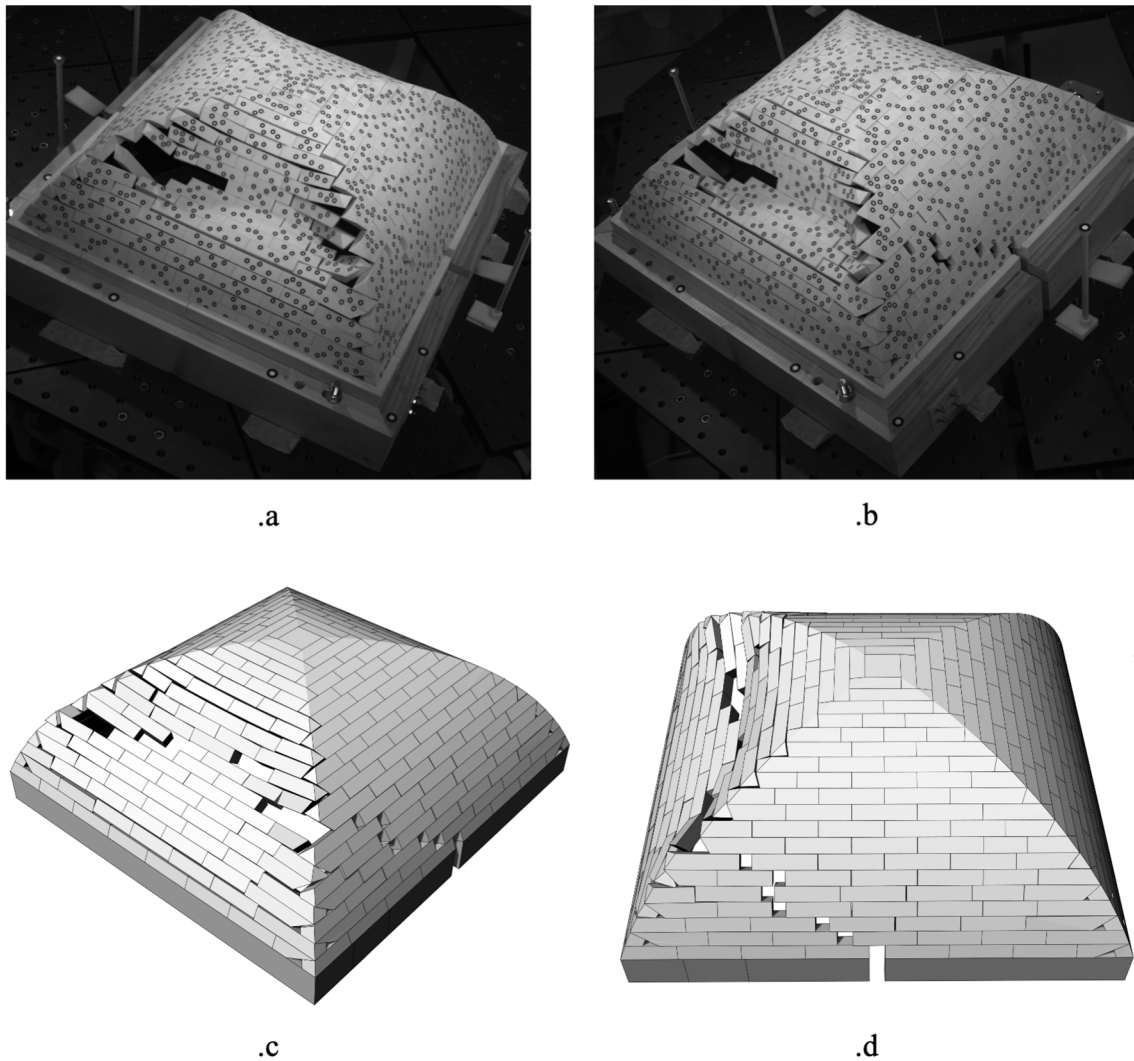


Fig. 19. Horizontal displacement of 1/2 of the support: (a) and (b) front view and lateral view of the physical model [37], (c) and (d) front view and lateral view of the numerical model in 3DEC with mechanical imperfections applied (friction angle 45 +/- 20%).

horizontal rows of voussoirs touch the edges, the contacts are no longer represented by face to face contacts, but by unpredictable vertex to face, vertex to edge or edge to edge contact typologies. The weakness of the newly formed contacts compromises the stability of the horizontal rows of blocks and consequently of the entire front web.

4. Results: Mechanical and geometrical imperfections

In this chapter, the results of the analyses with mechanical and geometrical imperfections will be depicted. In 4.1, the numerical

Table 3
Results of the 3DEC analyses conducted on the numerical model with geometrical imperfections (printer tolerance +/-0.1 mm).

Test (support displacement)	n of tests	Displacement capacity		Variation compared to [37]	Variation compared to perfect digital geometry
		Average value	Standard deviation		
1/2	20	3.43%	0.35%	+0.71%	+0.53%
1/4	10	3.36%	0.19%	+0.54%	-0.22%
1/8	10	3.70%	0.24%	+1.05%	+0.12%

analyses on the perfect digital geometry with mechanical imperfections will be presented. Finally, in 4.2, the results of the analyses conducted on the digital model with geometrical imperfections will be outlined, together with all the observed phenomena related to geometrical imperfections.

4.1. Role of mechanical imperfections

The application of mechanical imperfections has shown a certain effect on the displacement capacity of the numerical model of the pavilion vault. The results obtained assigning a different value of the friction angle at each block, picked inside a certain range, diverge from the results observed in the case of one unique value of the friction angle assigned to all the blocks (Table 2). For the tests with mechanical imperfections, the two joint stiffness values calculated using Eqs. (1) and (3) have been reduced by eight to reduce the computational time.

From a qualitative point of view, in the case of mechanical imperfections, the crack patterns observed were more similar to the one observed in [37] as shown in (Fig. 19a–d). Even if the exact distribution of the friction angles in a physical model is impossible to measure and replicate, the simulation of mechanical imperfections based on the friction angles and the standard deviation measured, showed a better approximation of the crack pattern observed in the physical model.

Table 4

Results of the 3DEC analyses conducted on the numerical model with geometrical imperfections (printer tolerance ± 0.1 mm + assembly errors 2% of block's length).

Test (support displacement)	n of tests	Displacement capacity		Variation compared to [37]	Variation compared to perfect digital geometry
		Average value	Standard deviation		
1/2	15	3.57%	0.39%	+0.85%	+0.67%
1/4	10	3.31%	0.22%	+0.49%	-0.27%
1/8	10	3.50%	0.20%	+0.85%	-0.08%

4.2. Role of geometrical imperfections

All real structures have geometrical imperfections, which can be caused by fabrication deviations, material placement errors or damages. In [Table 3](#) and [Table 4](#), the results of the analyses conducted in 3DEC on the numerical model with geometrical imperfections are presented. [Table 3](#) shows the results of the numerical model with fabrication deviations (in this work it corresponds to a printer tolerance equal to ± 0.1 mm), with friction angle 45 and joint stiffness values reduced by a factor of 16. [Table 4](#) shows the results of the numerical model with fabrication imperfections (printer tolerance equal to ± 0.1 mm) and assembly errors ($\pm 2\%$ of the block's longest side), with friction angle 45 and joint stiffness values reduced by a factor of 16.

In the appendix, [Table 5](#) shows a full overview of the results obtained in 3DEC on the numerical model with geometrical imperfections. The results presented in [Table 3](#) and [Table 4](#) show that geometrical imperfections also influence the displacement capacity. On average, the displacement capacity with the application of imperfections is higher compared to the

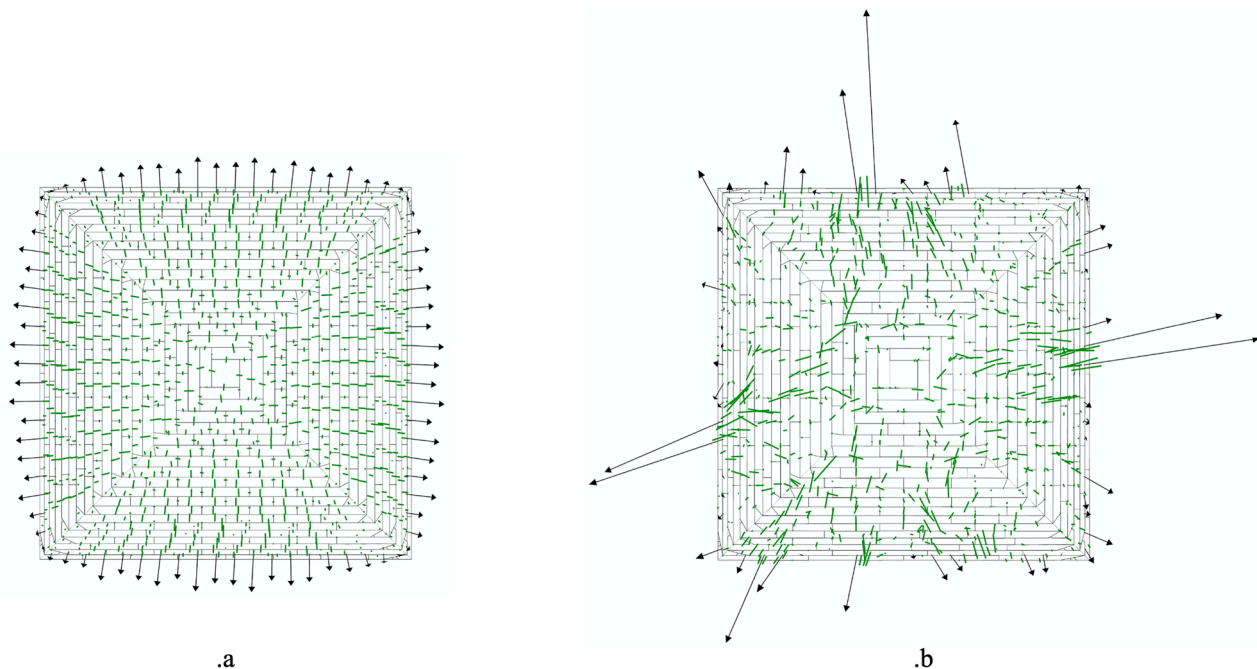


Fig. 20. Flow of forces in the numerical model used for the comparison with [37]. (a) resultant contact forces in green in the model with perfect geometry and resultants on the supports (grey arrows), (b) resultant contact forces in green in the model with geometrical imperfections and resultants on the supports (grey arrows). (For interpretation of the references to colour in this figure legend, the reader is referred to the web version of this article.)

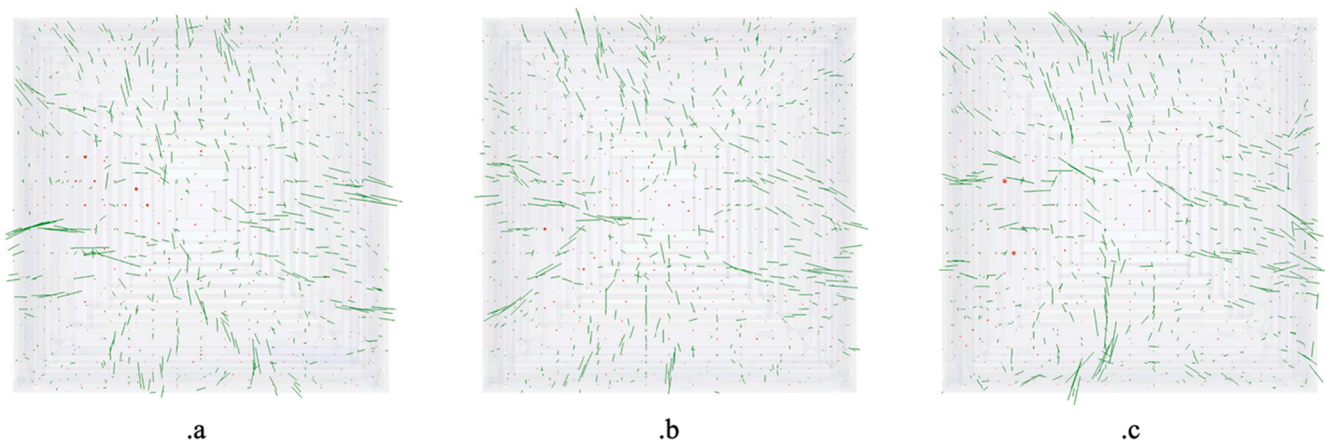


Fig. 21. Plan view of the flow of forces in three numerical models (a, b, c) with imperfections randomly generated considering only ± 0.1 mm material tolerance.

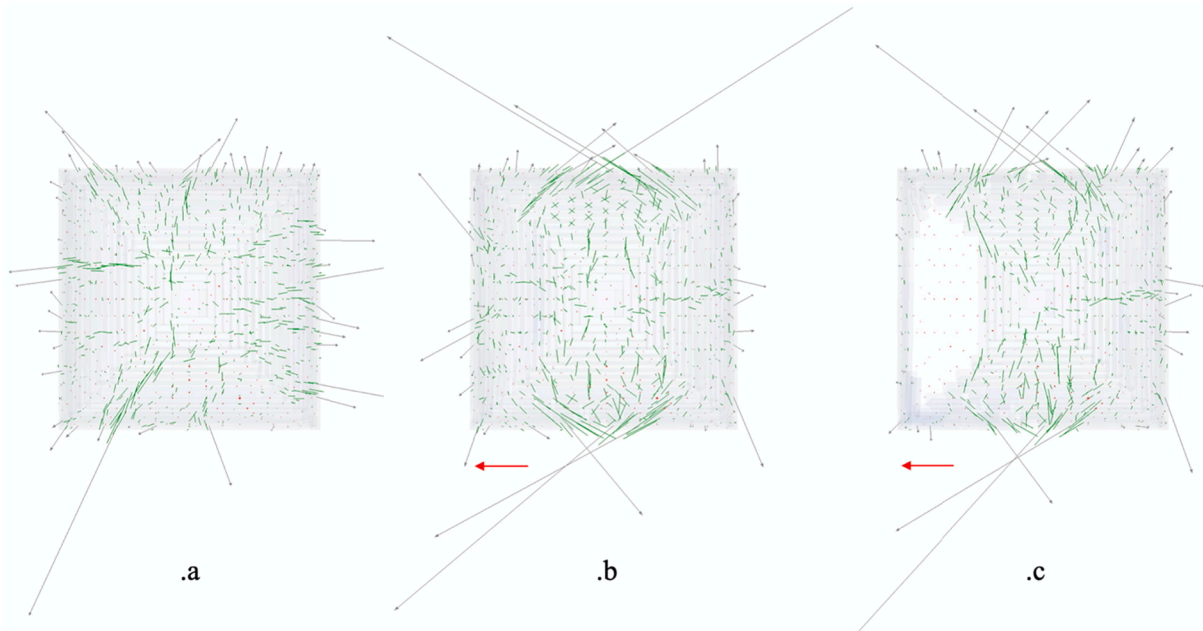


Fig. 22. Plan view of the flow of forces in three steps of the analysis on the same numerical model. (a) just gravity applied, (b) displacement equal to 1.5% of the vault's span, (c) after the collapse.

model without imperfections, but the standard deviation is also higher, meaning that the models with imperfections have more uncertainty than the model with perfect geometry.

To better understand how they influence the structure, the flow of forces has been studied during the analysis. After the application of geometrical imperfections, the initial configuration of the flow-of-forces changes entirely. Fig. 20.a represents the flow of forces and the

resultants on the supports in the perfect geometry, while Fig. 20b shows the flow of forces and the resultants on the supports in the case of geometrical imperfections (printer tolerance ± 0.1 mm). In 20.a, with perfect geometry, the structural behaviour is a combination of areas (central part of the web) where the forces flow bi-dimensionally down (single curvature), and areas close to the edges where the flow of forces deviates (double curvature). This combination influences the thrust

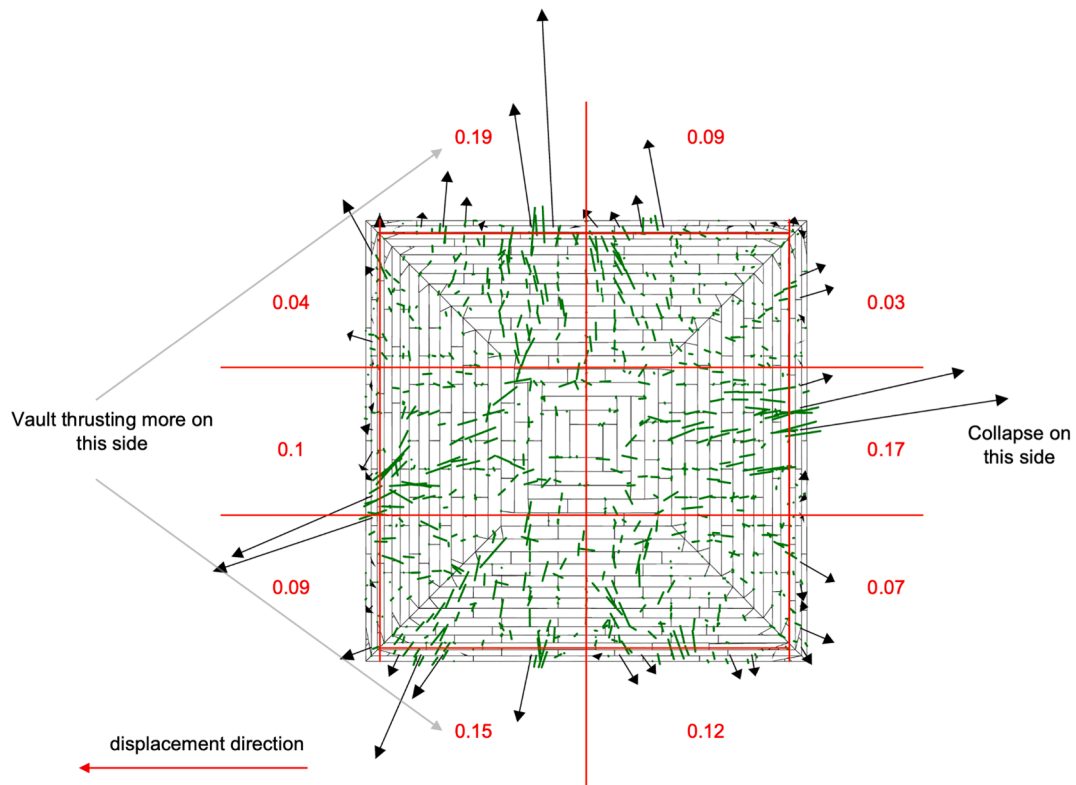


Fig. 23. Distribution of the vault's weight on the supports after application of gravity. Each number in the red oval indicates the amount of weight carried by the portion of the support in that area. (For interpretation of the references to colour in this figure legend, the reader is referred to the web version of this article.)

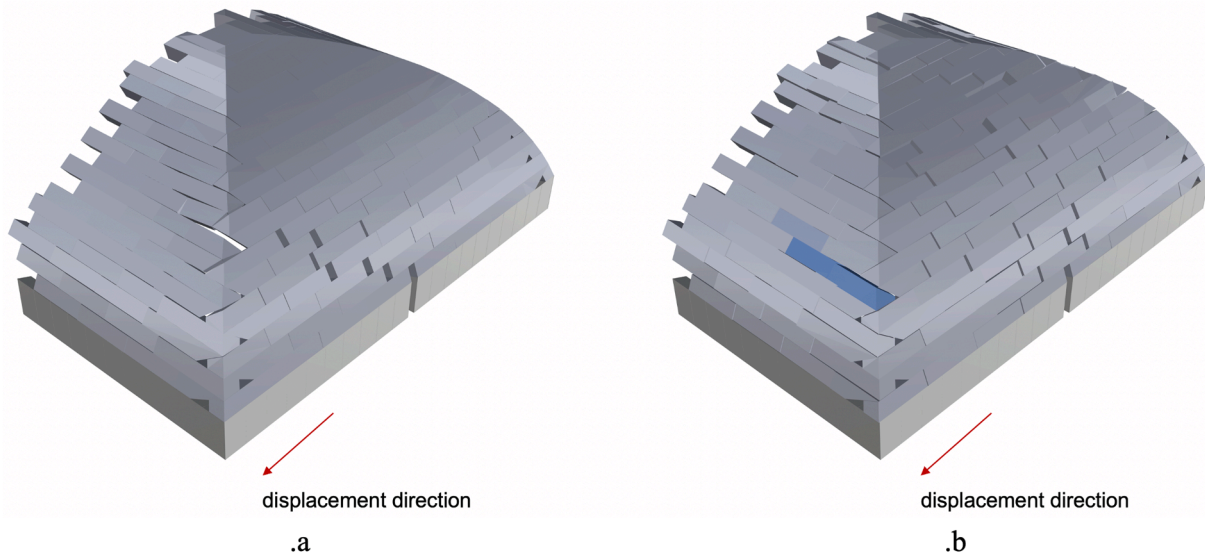


Fig. 24. Lateral web in the case of perfect geometry (a) and in the case of geometrical imperfections (b).

distribution on the supports, that goes from maximum value at the centre of the supports to a minimum value at the corners. The application of geometrical imperfections modifies the way the forces flow in the vault, and it also influences the distribution of the thrust on the supports.

Fig. 21 shows three different cases generated with a small amount of imperfections (printer tolerance ± 0.1 mm). Imperfections redirect the forces inside the structures, creating three different flows.

After the application of the displacement, the force distribution is influenced mainly by the support movement. As in the case of perfect geometry, the forces start flowing towards the lateral webs, and the lateral supports carry most of the vault's weight. In Fig. 22, the evolution of the flow of forces from the initial step until collapse can be observed. The initial flow, due to the applied imperfections, has a particular influence on the following force distributions.

The effect of the initial force distribution, due to imperfections, showed an influence in the analyses with the displacement of $\frac{1}{2}$ of the

supports. In fact, in these cases, the collapses happened 50% of the time on the front web and 50% on the back web. The reason for this phenomenon is related to the symmetry of this configuration and the imperfections. In fact, in all the analyses with perfect geometry, this never happened; consistently, the front web collapsed. In order to understand how and why imperfections could influence on which side the collapse happens, the distribution of the resultant forces on the supports has been investigated at the initial step, when only gravity is applied without displacements, and the flow of forces is influenced only by the imperfections and not by the horizontal displacement. This study showed that after the application of imperfections, the flow of forces changes and the weight of the pavilion vault was distributed in an asymmetric way between the left and right side, as visible in the model shown in Fig. 23. Consistently the collapse happened on the half of the support that carried less weight of the vault (i.e. lower magnitude of the normal forces and consequently smaller shear strength).

Table 5
Displacement capacity of the numerical model with geometrical imperfections.

Displacement/span %			Model										Average [%]	St. Dev [%]								
Support displ	Printer Tolerance [mm]	Translation [%]	[%]																			
1/2	0.1	0	M1	M2	M3	M4	M5	M6	M7	M8	M9	M10	3.43	0.35								
			3.24	3.24	2.90	3.58	3.24	3.24	3.07	3.58	3.92	3.58										
1/2	0.1	0	M11	M12	M13	M14	M15	M16	M17	M18	M19	M20	3.57	0.39								
			3.24	3.24	4.10	3.75	3.24	3.41	3.41	4.26	3.07	3.07										
1/2	0.1	2	T1	T2	T3	T4	T5	3.92	3.24	3.07	3.92	4.10	3.57	0.39								
			M1	M1	M1	M1	M1															
1/2	0.1	2	M11	M11	M11	M11	M11	M11	M11	M11	M11	M11	3.07	3.41	3.41	3.07	4.43	3.41	3.75	3.75	3.41	3.58
			T1	T2	T3	T4	T5	T6	T7	T8	T9	T10										
1/4	0.1	0	M1	M2	M3	M4	M5	M6	M7	M8	M9	M10	3.36	0.19								
			3.58	3.07	3.41	3.58	3.58	3.24	3.41	3.07	3.41	3.24										
1/4	0.1	2	M1	M1	M1	M1	M1	M1	M1	M1	M1	M1	3.31	0.22								
			T1	T2	T3	T4	T5	T6	T7	T8	T9	T10										
1/8	0.1	0	M1	M2	M3	M4	M5	M6	M7	M8	M9	M10	3.70	0.24								
			3.75	3.24	3.75	3.75	3.92	3.41	4.10	3.58	3.92	3.58										
1/8	0.1	2	M1	M1	M1	M1	M1	M1	M1	M1	M1	M1	3.50	0.20								
			T1	T2	T3	T4	T5	T6	T7	T8	T9	T10										
			3.58	3.58	3.41	3.07	3.41	3.41	3.58	3.92	3.41	3.58										

Another effect due to imperfections is the dissipation of the displacement applied. In the perfect geometry, at the start of the displacement, the cracks on the lateral webs appear, and the corner edges open up (Fig. 24a). With geometrical imperfections because of the non-perfect contacts between the blocks, the horizontal support displacement often caused more distributed cracks along the lateral webs (Fig. 24b), i.e. more cracks opened up, and the effect on the corner edges is reduced. This effect, in some cases, contributed to the increase of the displacement capacity because the joints at the edges started to opening a few steps later than usual.

As a general effect, imperfections cause the localisation of the flow of forces. The theoretical face-to-face contacts become vertex-to-face, vertex-to-edge, edge-to-edge or edge-to-face contacts. Localisation directs forces in specific directions, but also often caused joint openings to be more distributed. As a result, the displacement capacity of the pavilion vault could slightly increase or decrease.

5. Conclusion

This paper focuses on the comparison between the tests conducted in [37] on the physical scale model of a pavilion vault subjected to horizontal displacement of the support and the computational analyses conducted on its digital version using the DEM software 3DEC by Itasca. The computational analysis has been conducted not only using the perfect digital model of the pavilion vault tested in [37] but also modelling mechanical and geometrical imperfections to understand their influence on the structural behaviour. The Python-based package *compas_assembly* has been used to manage the entire geometry, to generate imperfections, and to post-process the results given by 3DEC, both for the computation and visualisation of the flow of forces within the structure and for the collapse detection.

As a first conclusion, the sensitivity analysis conducted on the joint stiffness values required by 3DEC for the calculation of the contact forces showed that their reduction in a certain range decreases the computational time up to 85% without altering the results.

The results on the “perfect” numerical model showed good agreement in terms of displacement capacity (slightly larger), crack patterns and collapse mechanisms compared to [37] (see Table 1). Only small differences can be seen in the location of the hinges just before the collapse.

The visualisation of the flow of forces within the perfect numerical model, no subjected to horizontal displacement of the support, showed how the geometry influences the structural behaviour of the pavilion vault in the initial configuration. In particular, the internal stress state was characterized by forces flowing bi-dimensionally down (single curvature) in the central area of the webs, and forces that deviate close to the edges (double curvature) where the magnitudes of the shear forces increased. On the supports, the combination of the two effects influences the thrust distribution that, as shown in Fig. 20a, goes from maximum value at the centre of the supports to a minimum value at the corners.

The introduction of mechanical imperfections did not show a significant variation of the results concerning the displacement capacity (slightly larger than the model with no imperfections). Still, the observed collapse behaviour is qualitatively more similar to the one in the real scale model (see Fig. 19). The modelling of mechanical imperfections implemented in this paper can be further employed to investigate the influence of not constant distributions of mechanical parameters, especially within historic masonry structures.

The application of geometrical imperfections belonging to each real structure, developed in this work, represents another layer of uncertainty that could lead to the localisation of forces, local cracks, unpredictable interlocking and variation in the distribution of shear strength. The geometrical imperfections modified the internal stress state of the structure in its initial configuration, affected the distribution of the thrust on the supports, and influenced the displacement capacity that slightly increased compared to the model with perfect geometry. Even

when the applied support displacement reduces the level of indeterminacy of the structure, and dominates the internal stress state, the modified starting configuration due to the imperfections still had an influence on the evolution of the force flow. Geometrical imperfections dissipated the effect of the displacement allowing the opening of more but smaller cracks.

More generally, the analyses confirmed the reliability of the DEM method for the study of URM structures, and the paper proposes a new strategy to model mechanical and geometrical imperfections and to test several various assumptions. Thanks to the newly implemented workflow and the visualisation of the flow of forces, it is now possible to follow the collapse also from a structural, i.e. force equilibrium, point of view and not only geometrically. The description of the three-dimensional evolution of the collapse, with the opening of the cracks and the relation between them, could be useful in practice for recognising damages caused by displacements of the supports.

Funding

This work was supported by the SNSF - Swiss National Science Foundation. Project grant n 178953: “Practical Stability Assessment Strategies for Vaulted Unreinforced Masonry Structures”.

CRediT authorship contribution statement

Alessandro Dell'Endice: Conceptualization, Methodology, Software, Formal analysis, Investigation, Data curation, Writing - original draft, Writing - review & editing, Visualization. **Antonino Iannuzzo:** Conceptualization, Validation, Software, Writing - review & editing. **Matthew J. DeJong:** Resources, Supervision, Validation, Writing - review & editing. **Tom Van Mele:** Conceptualization, Resources, Supervision, Validation, Software, Writing - review & editing, Funding acquisition. **Philippe Block:** Conceptualization, Resources, Supervision, Validation, Writing - review & editing, Funding acquisition.

Declaration of Competing Interest

The authors declare that they have no known competing financial interests or personal relationships that could have appeared to influence the work reported in this paper.

Acknowledgement

The first author would like to thank Prof. Tomás Méndez Echenagucia for his valuable support in the parametric modelling of the geometry, and Dr. Michela Rossi for her support and advises at the beginning of this work.

Appendix

In this appendix is presented a full overview of the analysis on the numerical model with geometrical imperfections. Table 5 shows the results in terms of mean value of the displacement capacity and standard deviation.

References

- [1] Heyman J. The stone skeleton. *Int J Solids Struct* 1966. [https://doi.org/10.1016/0020-7683\(66\)90018-7](https://doi.org/10.1016/0020-7683(66)90018-7).
- [2] Huerta S. *Mechanics of masonry vaults: The equilibrium approach*. 3rd Int Semin Hist Constr Guimarães. Port 2001.
- [3] Huerta S. The Analysis of Masonry Architecture: A Historical Approach. *Archit Sci Rev* 2009. <https://doi.org/10.3763/asre.2008.5136>.
- [4] Zessin J, Lau W, Ochsendorf J. Equilibrium of cracked masonry domes. *Proc Inst Civ Eng Eng Comput Mech* 2010. <https://doi.org/10.1680/eacm.2010.163.3.135>.
- [5] Block P. *Thrust Network Analysis: Exploring Three-dimensional Equilibrium*. PhD Thesis 2009.

- [6] Block P, Lachauer L. Three-dimensional (3D) equilibrium analysis of gothic masonry vaults. *Int. J. Archit. Herit.* 2014. <https://doi.org/10.1080/15583058.2013.826301>.
- [7] Fraternali F, Angelillo M, Fortunato A. A lumped stress method for plane elastic problems and the discrete-continuum approximation. *Int J Solids Struct* 2002. [https://doi.org/10.1016/S0020-7683\(02\)00472-9](https://doi.org/10.1016/S0020-7683(02)00472-9).
- [8] Fraternali F. A thrust network approach to the equilibrium problem of unreinforced masonry vaults via polyhedral stress functions. *Mech Res Commun* 2010. <https://doi.org/10.1016/j.mechrescom.2009.12.010>.
- [9] Angelillo M, Babilio E, Fortunato A. Singular stress fields for masonry-like vaults. *Contin Mech Thermodyn* 2013. <https://doi.org/10.1007/s00161-012-0270-9>.
- [10] Angelillo M, Fortunato A. Equilibrium of masonry vaults. *Lect Notes Appl Comput Mech* 2004. <https://doi.org/10.1007/978-3-540-45287-4>.
- [11] Iannuzzo A. A New RIGID BLOCK MODEL FOR MASONRY STRUCTURES. Università degli Studi di Napoli Federico II, 2017.
- [12] Iannuzzo A, Van Mele T, Block P. Piecewise rigid displacement (PRD) method: a limit analysis-based approach to detect mechanisms and internal forces through two dual energy criteria. *Mech Res Commun* 2020. <https://doi.org/10.1016/j.mechrescom.2020.103557>.
- [13] Iannuzzo A, Dell'Endice A, Van Mele T, Block P. Numerical Limit Analysis-based modelling of masonry structures subjected to large displacements. *Comput Struct* 2020. <https://doi.org/10.1016/j.compstruc.2020.106372>.
- [14] D'Ayala D, Casapulla C. Limit state analysis of hemispherical domes with finite friction. *Struct Anal Hist Constr* 2001;617–26. 972-8692-01-3.
- [15] Orduña A, Lourenço PB. Three-dimensional limit analysis of rigid blocks assemblages. Part I: Torsion failure on frictional interfaces and limit analysis formulation. *Int J Solids Struct* 2005. <https://doi.org/10.1016/j.ijsolstr.2005.02.010>.
- [16] Portioli F, Casapulla C, Gilbert M, Cascini L. Limit analysis of 3D masonry block structures with non-associative frictional joints using cone programming. *Comput Struct* 2014. <https://doi.org/10.1016/j.compstruc.2014.07.010>.
- [17] Mousavian E, Casapulla C. The role of different sliding resistances in limit analysis of hemispherical masonry domes. *Frat Ed Integrita Strutt* 2020. <https://doi.org/10.3221/IGF-ESIS.51.25>.
- [18] Cundall PA. A computer model for simulating progressive large-scale movements in blocky rock systems. *Proceedings Symp. Int. Soc. Rock Mech. Nancy 2 1971*:8.
- [19] Lemos J. DISCRETE ELEMENT MODELING OF MASONRY STRUCTURES 2007; 3058. doi:10.1080/15583050601176868.
- [20] DeJong MJ. Seismic Assessment Strategies for Masonry Structures. 2009.
- [21] Simon J, Bagi K. Discrete Element Analysis of the Minimum Thickness of Oval Masonry Domes. *Int J Archit Herit* 2016. <https://doi.org/10.1080/15583058.2014.996921>.
- [22] Lemos JV. Discrete element modelling of the seismic behaviour of stone masonry arches. *Fourth Int Symp Comput Methods Struct Mason* 1998:220–7.
- [23] Çaktı E, Saygılı Ö, Lemos JV, Oliveira CS. Discrete element modeling of a scaled masonry structure and its validation. *Eng Struct* 2016. <https://doi.org/10.1016/j.engstruct.2016.07.044>.
- [24] Lemos JV. Modelling the dynamics of masonry structures with discrete elements. *Open Constr Build Technol J* 2016;10:210–9. <https://doi.org/10.2174/1874836801610010210>.
- [25] Dimitri R, De Lorenzis L, Zavarise G. Numerical study on the dynamic behavior of masonry columns and arches on buttresses with the discrete element method. *Eng Struct* 2011. <https://doi.org/10.1016/j.engstruct.2011.08.018>.
- [26] McInerney J, DeJong MJ. Discrete Element Modeling of Groin Vault Displacement Capacity. *Int J Archit Herit* 2015. <https://doi.org/10.1080/15583058.2014.923953>.
- [27] Alexakis H, Makris N. Validation of the Discrete Element Method for the Limit Stability Analysis of Masonry Arches, 2016, p. 292–325. doi:10.4018/978-1-5225-0231-9.ch012.
- [28] Lengyel G. Discrete element analysis of gothic masonry vaults for self-weight and horizontal support displacement. *Eng Struct* 2017. <https://doi.org/10.1016/j.engstruct.2017.06.014>.
- [29] Sarhosis V, Lemos JV, Bagi K. Discrete element modeling. *Numer Model Mason Hist Struct Elsevier* 2019:469–501. <https://doi.org/10.1016/b978-0-08-102439-3.00013-0>.
- [30] DeJong MJ, Vibert C. Seismic response of stone masonry spires: Computational and experimental modeling. *Eng Struct* 2012. <https://doi.org/10.1016/j.engstruct.2012.03.001>.
- [31] Van Mele T, McInerney J, DeJong MJ, Block P. Physical and Computational Discrete Modelling of Masonry Vault Collapse. *Struct Anal Hist Constr* 2012;1–3: 2552–60.
- [32] Caddemi S, Calìo I, Cannizzaro F, Occhipinti G, Pantò B. A parsimonious discrete model for the seismic assessment of monumental structures. *Civil-Comp Proc.* 2015. <https://doi.org/10.4203/ccp.108.82>.
- [33] Cannizzaro F, Pantò B, Caddemi S, Calìo I. A Discrete Macro-Element Method (DMEM) for the nonlinear structural assessment of masonry arches. *Eng Struct* 2018. <https://doi.org/10.1016/j.engstruct.2018.04.006>.
- [34] Danyzy AAH. Méthode générale pour déterminer la résistance qu'il faut opposer à la poussée des voûtes. *Hist La Société R Des Sci Établie à Montpellier 1732*;2:1778.
- [35] Frezier A-F. La théorie et la pratique de la coupe des pierres et des bois, pour la construction des voûtes... ou Traité de stéréotomie à l'usage de l'architecture. Jean-Daniel Doulsseker 1737;.1.
- [36] Addis B. Physical modelling and form finding. *Shell Struct. Archit. Form Find. Optim.* 2014. <https://doi.org/10.4324/9781315849270>.
- [37] Rossi M, Calvo Barentin C, Van Mele T, Block P. Experimental study on the behaviour of masonry pavilion vaults on spreading supports. *Structures* 2017;11. <https://doi.org/10.1016/j.istruc.2017.04.008>.
- [38] Calvo Barentin C, Van Mele T, Block P. Robotically controlled scale-model testing of masonry vault collapse. *Meccanica* 2018;53:1917–29. <https://doi.org/10.1007/s11012-017-0762-6>.
- [39] Heyman J. The structural engineer's view of ancient buildings. *J Mech Mater Struct* 2018;13:609–15. <https://doi.org/10.2140/JOMMS.2018.13.609>.
- [40] Bigoni D, Noselli G. Localized stress percolation through dry masonry walls. Part I - Experiments. *Eur J Mech A/Solids* 2010. <https://doi.org/10.1016/j.euromechsol.2009.10.009>.
- [41] Bigoni D, Noselli G. Localized stress percolation through dry masonry walls. Part II - Modelling. *Eur J Mech A/Solids* 2010. <https://doi.org/10.1016/j.euromechsol.2009.10.013>.
- [42] Chewe Ngapeya GG, Waldmann D, Scholzen F. Impact of the height imperfections of masonry blocks on the load bearing capacity of dry-stack masonry walls. *Constr Build Mater* 2018. <https://doi.org/10.1016/j.conbuildmat.2017.12.183>.
- [43] Le TE. *volte in muratura negli edifici storici: tecniche costruttive e comportamento strutturale.* Italy (in Italian): University of Trento; 2008.
- [44] Itasca Consulting Group I. 3DEC — Three-Dimensional Distinct Element Code, Ver. 5.2. Minneapolis: Itasca 2016.
- [45] Cundall PA. Formulation of a three-dimensional distinct element model-Part I. A scheme to detect and represent contacts in a system composed of many polyhedral blocks. *Int J Rock Mech Min Sci* 1988. [https://doi.org/10.1016/0148-9062\(88\)92293-0](https://doi.org/10.1016/0148-9062(88)92293-0).
- [46] Hart R, Cundall PA, Lemos J. Formulation of a three-dimensional distinct element model-Part II. Mechanical calculations for motion and interaction of a system composed of many polyhedral blocks. *Int J Rock Mech Min Sci* 1988. [https://doi.org/10.1016/0148-9062\(88\)92294-2](https://doi.org/10.1016/0148-9062(88)92294-2).
- [47] Van Mele T, Liew A, Méndez Echenagucia T, Rippmann M. COMPAS: A framework for computational research in architecture and structures 2017.
- [48] Sarhosis V. Micro-Modeling Options for Masonry, 2016. doi:10.4018/978-1-5225-0231-9.ch002.